Applied Physics Letters

Large spin Hall effect and increase in perpendicular magnetic anisotropy in artificially synthesized amorphous W/Hf multilayer/CoFeB system

Cite as: Appl. Phys. Lett. **116**, 132401 (2020); https://doi.org/10.1063/5.0002642
Submitted: 26 January 2020 . Accepted: 12 March 2020 . Published Online: 30 March 2020

Yoshiaki Saito, Nobuki Tezuka, Shoji Ikeda, and Tetsuo Endoh

Applied Physics Letters ARTICLE scitation.org/journal/apl

Large spin Hall effect and increase in perpendicular magnetic anisotropy in artificially synthesized amorphous W/Hf multilayer/CoFeB system

Cite as: Appl. Phys. Lett. **116**, 132401 (2020); doi: 10.1063/5.0002642
Submitted: 26 January 2020 · Accepted: 12 March 2020 ·
Published Online: 30 March 2020

Yoshiaki Saito,[1,a] Nobuki Tezuka,[2,3] Shoji Ikeda,[1,3,4,5] and Tetsuo Endoh[1,3,4,5,6]

AFFILIATIONS

[1]Center for Innovative Integrated Electronic Systems, Tohoku University, Sendai 980-0845, Japan
[2]Department of Materials Science, Graduate School of Engineering, Tohoku University, Sendai 980-8579, Japan
[3]Center for Spintronics Research Network, Tohoku University, Sendai 980-8577, Japan
[4]Center for Science and Innovation in Spintronics, Tohoku University, Sendai 980-8577, Japan
[5]Research Institute of Electrical Communication, Tohoku University, Sendai 980-8577, Japan
[6]Department of Electrical Engineering, Graduate School of Engineering, Tohoku University, Sendai 980-8579, Japan

[a)]Author to whom correspondence should be addressed: ysaito@cies.tohoku.ac.jp

ABSTRACT

We studied the spin-Hall effect and perpendicular magnetic anisotropy in W/Hf multilayer/CoFeB/MgO and $W_{80}Ta_{20}$/Hf multilayer/CoFeB/MgO systems and compared them with those in the β-W/CoFeB/MgO system. From the cross-sectional high-resolution transmission electron microscopy images, (i) the amorphous structure of W/Hf and $W_{80}Ta_{20}$/Hf multilayers, (ii) the flat interface between heavy metals and CoFeB, and (iii) highly (100) texture of MgO (1.0 nm) on CoFeB were observed in those multilayer systems. A higher spin-Hall effect and enhancement of perpendicular magnetic anisotropy in the W/Hf multilayer/CoFeB/MgO system can be achieved compared to the β-W/CoFeB/MgO system. In addition, we found that the resistivity in amorphous W/Hf multilayers is low compared to that in β-W. These results suggest that the artificially synthesized multilayer system is one of the avenues for realizing the heavy metal with a large spin-Hall effect and low resistivity.

Current-induced spin–orbit torque (SOT) originating from the spin-Hall effect (SHE) in heavy metal/ferromagnet (HM/FM) systems has attracted attention due to their potential for application in the efficient manipulation of magnetization of nano-magnets in SOT magnetoresistive random access memory (SOT-MRAM), skyrmions, and domain wall devices.[1–16] For application to a large-scale integration, the efficient SOT operation (high spin Hall angle $|\theta_{SH}|$) in low resistivity (ρ_{xx}) HM is necessary.[17,18] Materials and HM/FM interfaces with larger spin–orbit coupling have been attracting interest because they allow a larger amount of spin current (J_s) to be generated for manipulating the magnetization when the write charge current (J_C) is passed through the HM layers. Magnitudes of $|\theta_{SH}| = |J_S/J_C|$ have been determined for various HMs by measuring the spin-Hall magnetoresistance (SMR) and spin torque ferromagnetic resonance (ST-FMR)[19–23] and by other means. W in which the crystalline structure is polycrystalline *A*15 (β-phase) or a mixture of β-phase and amorphous phase has large magnitudes of θ_{SH}.[1,12,19,20,23] Due to the extensive efforts, the efficiency of present SOT operations, that is, the absolute values of θ_{SH} ($|\theta_{SH}|$), becomes larger day by day; however, almost all HMs with a large magnitude of $|\theta_{SH}|$ have a very high resistivity (ρ_{xx}). For instance, β-W has a relatively large $|\theta_{SH}|$ of approximately 0.2–0.3 and, however, has very high resistivity ($\rho_{xx} \approx$ 200–300 $\mu\Omega$ cm); $|\theta_{SH}|$ generally reported for β-Ta and amorphous Hf (a-Hf) is approximately 0.1, and β-Ta and a-Hf also have very high resistivity ($\rho_{xx} \approx$ 200 and 400 $\mu\Omega$ cm, respectively).[1,12,20,23] The magnitude of $|\theta_{SH}|$ for both intrinsic and extrinsic (side jump mechanism) terms is proportional to the

magnitude of the ρ_{xx} value ($|\theta_{SH}| \sim \sigma_{SH}\ \rho_{xx}$[24,25]), where σ_{SH} is the spin Hall conductivity. Therefore, the increase in the magnitude of σ_{SH} would be important from the application point of view.

In this paper, we propose a HM with an artificially synthesized amorphous W/Hf multilayer in which we observed a large magnitude of σ_{SH} and low ρ_{xx} compared to those in β-W.

We prepared Ta(0.5)/W(t_{HM})/CoFeB(t_{CoFeB})/MgO(1.0)/Ta(1), Ta(0.5)/artificially synthesized $(W(0.35)/Hf(0.35))_n$ multilayer(t_{HM})/CoFeB(t_{CoFeB})/MgO(1.0)/Ta(1) (n: repetition number), Ta(0.5)/$(W(0.7)/Hf(0.7))_n$ multilayer(t_{HM})/CoFeB(t_{CoFeB})/MgO(1.0)/Ta(1), and Ta(0.5)/$(W_{80}Ta_{20}(0.7)/Hf(0.7))_n$ multilayer(t_{HM})/CoFeB(t_{CoFeB})/MgO(1.0)/Ta(1) systems with various HM and CoFeB thicknesses (t_{HM} and t_{CoFeB}, respectively) on high resistive Si substrates, where numbers in the parentheses indicate the nominal thickness in nm. These systems with various t_{HM} values (=1.5–7.0 nm) are patterned into the microscale Hall bar by photolithography and Ar ion milling. The detailed fabrication process was described in the previous paper.[17] The processed wafers were then annealed at 573 K in vacuum less than 1×10^{-4} Pa for an hour. The inset in Fig. 1(e) shows the schematic diagram of the devices and the typical device photograph. The SHE in these devices with various t_{HM} values was measured at 305 K by means of SMR. For the measurements of SMR, the current, which is less than or equal to 5 μA, is passed through the devices in the x-axis direction as shown in the inset in Fig. 1(e) and an external magnetic field between −4 and +4 Tesla is applied to both the y- and z-axis directions. Magnetic properties were measured by using a vibrating sample magnetometer (VSM) at 298 K.

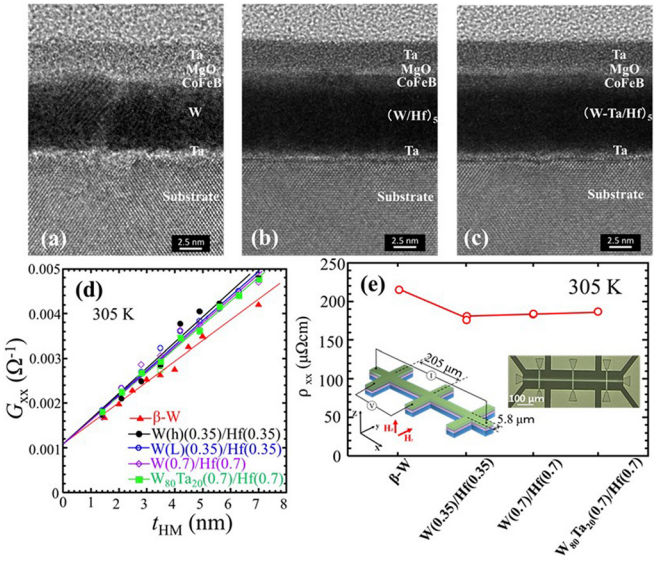

FIG. 1. Cross-sectional high-resolution transmission electron microscopy images of (a) Ta(0.5)/W(7)/CoFeB(1.5)/MgO(1.0)/Ta(1), (b) Ta(0.5)/$(W(0.7)/Hf(0.7))_5$ multilayer/CoFeB(1.5)/MgO(1.0)/Ta(1), and (c) Ta(0.5)/$(W_{80}Ta_{20}(0.7)/Hf(0.7))_5$ multilayer/CoFeB(1.5)/MgO(1.0)/Ta(1) systems, where numbers in the parentheses show the nominal thickness in nm. (d) shows sheet conductance (G_{xx}) as a function of HM thickness (t_{HM}). The solid lines in (d) are linear fits to the data. (e) shows the estimated resistivity (ρ_{XX}) from the fits in (d).

The film structures for all systems with $t_{HM} = 7$ nm were investigated by x-ray diffraction (XRD) and cross-sectional high-resolution transmission electron microscopy (HR-TEM). Figures 1(a)–1(c) show the typical HR-TEM images for Ta(0.5)/W(7)/CoFeB(1.5)/MgO(1.0)/Ta(1), Ta(0.5)/$(W(0.7)/Hf\ (0.7))_5$ multilayer/CoFeB(1.5)/MgO(1.0)/Ta(1), and Ta(0.5)/$(W_{80}Ta_{20}(0.7)/Hf(0.7))_5$ multilayer/CoFeB(1.5)/MgO(1.0)/Ta(1) systems annealed at 573 K, respectively. The results show that the W structure has polycrystalline $A15$ (β-phase) and all artificially synthesized W/Hf and $W_{80}Ta_{20}$/Hf multilayers have an amorphous structure. For the Ta(0.5)/$(W(0.7)/Hf(0.7))_5$ multilayer/CoFeB(1.5)/MgO(1.0)/Ta(1) system, we confirmed that the W/Hf multilayer film has an amorphous structure even after annealing at 673 K. For the sputtering Ar gas pressure (P_{Ar}) for W in W/Hf and $W_{80}Ta_{20}$/Hf multilayers, we used two different conditions of $P_{Ar} = 2.55$ Pa and $P_{Ar} = 0.39$ Pa, which are β- and a-phase preparation conditions in previous W deposition,[17] respectively. In the W/Hf and $W_{80}Ta_{20}$/Hf multilayers we prepared here, there is no difference in the amorphous structures of W/Hf and $W_{80}Ta_{20}$/Hf multilayers for the different P_{Ar} conditions. From the HR-TEM images, it is found that a flat interface between HMs and CoFeB and highly (100) texture of MgO (1.0 nm) on CoFeB were observed in the multilayer systems [Figs. 1(b) and 1(c)], whereas the rough interface between β-W and CoFeB and not clear texture of MgO (1.0 nm) on CoFeB were observed in the β-W(7)/CoFeB (1.5)/MgO(1.0) system [Fig. 1(a)]. The flat interface between HMs and CoFeB and highly (100) texture of MgO (1.0 nm) on CoFeB were also observed for the $(W(0.7)/Hf(0.7))_5$/CoFeB/MgO/Ta system annealed at 673 K.

Figure 1(d) shows the inverse of the device longitudinal resistance ($1/R_{xx}$) multiplied by a geometrical factor (L/w), and the sheet conductance, $G_{xx} = L/(wR_{xx})$, values are plotted as a function of the HM layer thickness (t_{HM}) in β-W, W(h)(0.35)/Hf(0.35), W(L)(0.35)/Hf(0.35), W(0.7)/Hf(0.7), and $W_{80}Ta_{20}(0.7)$/Hf(0.7) multilayer systems, where $L = 205$ μm and $w = 5.8$ μm as shown in the inset of Fig. 1(e). W (h) and W (L) are tungsten (W) films prepared at high (h) pressure ($P_{Ar} = 2.55$ Pa) and low (L) pressure ($P_{Ar} = 0.39$ Pa) conditions, respectively. The G_{xx} values are also nearly the same between artificially synthesized W(h)(0.35)/Hf(0.35) and W(L)(0.35)/Hf(0.35) multilayers prepared at $P_{Ar} = 2.55$ Pa and $P_{Ar} = 0.39$ Pa as shown in Fig. 1(d). The ρ_{xx} values for all multilayer systems are also nearly the same for the multilayers prepared at $P_{Ar} = 2.55$ Pa and $P_{Ar} = 0.39$ Pa because of having the same amorphous structure, and therefore, from here, we do not distinguish between W(h) and W(L). Since the slope in Fig. 1(d) is the inverse of the resistivity of HM ($1/\rho_{xx}$), Fig. 1(d) shows that the resistivity ρ_{xx} values for multilayer systems are smaller than that for β-W. Figure 1(e) shows the resistivity ρ_{xx} values fitted by the least squares method for all these systems. Thus, we found that the ρ_{xx} values in amorphous W/Hf and $W_{80}Ta_{20}$/Hf multilayers are low compared to that in β-W. Metastable polycrystalline β-phase W has a higher resistivity compared to amorphous W/Hf and $W_{80}Ta_{20}$/Hf multilayers. Note that the resistivity of the amorphous multilayers is higher than that of stable α-phase W.[17]

Figure 2(a) shows the t_{CoFeB} dependence of effective magnetic anisotropy energy ($K_{eff}t^*$). $K_{eff} = K_b - M_S^2/2\mu_0 + 2K_i/t^*$ and $t^* = t_{CoFeB} - t_{dead}$, where K_b is the bulk crystalline anisotropy, K_i is the interfacial anisotropy, $(-M_S^2/2\mu_0)$ is the demagnetization, M_S is the saturation magnetization, μ_0 is the permeability of vacuum, and t_{dead} is the magnetic dead layer thickness. As shown in Fig. 2(b), since the x-axis

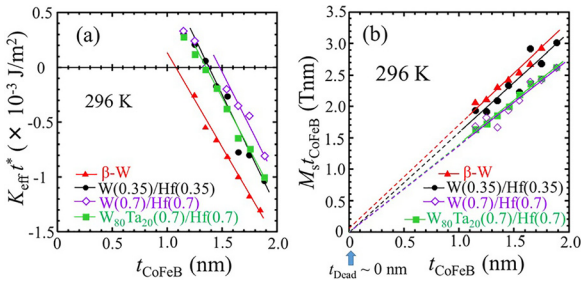

FIG. 2. CoFeB thickness (t_{CoFeB}) dependence of (a) effective magnetic anisotropy energy ($K_{eff}\,t^*$) and (b) multiplication of saturation magnetization (M_S) and t_{CoFeB} for Ta/W(7)/CoFeB(t_{CoFeB})/MgO(1.0)/Ta(1), Ta/(W(0.7)/Hf(0.7))$_5$ multilayer/CoFeB(t_{CoFeB})/MgO(1.0)/Ta(1), and Ta/($W_{80}Ta_{20}$(0.7)/Hf(0.7))$_5$ multilayer/CoFeB(t_{CoFeB})/MgO(1.0)/Ta(1) systems.

intercept in Fig. 2(b) is nearly zero, we confirmed $t_{dead} = 0$. Therefore, $K_{eff}\,t^* = K_{eff}\,t_{CoFeB}$. From the y-axis intercept in Fig. 2(a), it is found that K_i values are 0.92, 1.43, 1.47, and 1.28 [$\times 10^{-3}$ J/m^2] for β-W, W(0.35)/Hf(0.35), W(0.7)/Hf(0.7), and $W_{80}Ta_{20}$(0.7)/Hf(0.7) multilayer systems, respectively. Thus, we found the enhancement of perpendicular magnetic anisotropy in artificially synthesized W/Hf and $W_{80}Ta_{20}$/Hf multilayer/CoFeB/MgO systems compared to that in β-W/CoFeB/MgO systems. In the cross-sectional HR-TEM images, the flat interface between HM and CoFeB and highly (100) texture of MgO (1.0 nm) on CoFeB were observed in those amorphous multilayer systems as described before. Moreover, we confirmed that there are no significant changes in K_i values and $t_{dead} = 0$ behavior even for all multilayers annealed at 673 K. The flat interface, highly MgO(100) texture, and Hf interface[26] would be the origin of $K_{eff}\,t^*$ enhancement.

Figures 3(a) and 3(b) show the typical longitudinal resistance (R_{xx}) vs external magnetic field (H) measured at 305 K for the devices with amorphous W(0.7)/Hf(0.7) and amorphous $W_{80}Ta_{20}$(0.7)/Hf(0.7) multilayers, respectively. As shown in Figs. 3(a) and 3(b), the values of R_{xx} in the magnetic field directions along the z-axis, $H_z > 0$ T and $H_z < 0$ T, are nearly the same [for example, R_{xx} ($H_z = 4$ T) $\sim R_{xx}$ ($H_z = -4$ T)]; however, the values of R_{xx} in the magnetic field directions along the y-axis, $H_y > 0$ T and $H_y < 0$ T, are different from each other for both the devices with amorphous W(0.7)/Hf(0.7) and amorphous $W_{80}Ta_{20}$(0.7)/Hf(0.7) multilayers. For the devices with amorphous W(0.7)/Hf(0.7) multilayers, the value of R_{xx} at $H_y = 4$ T is smaller than that at $H_y = -4$ T [Fig. 3(a)], and for the devices with amorphous $W_{80}Ta_{20}$(0.7)/Hf(0.7) multilayers, the value of R_{xx} at $H_y = 4$ T is larger than that at $H_y = -4$ T [Fig. 3(b)]. These are related to the anomalous Nernst voltage (V_{Nernst}) due to the thermal hot electron current flow from the film to the high resistive Si substrate as discussed in Ref. 17 and imply that the sign of V_{Nernst} is different between W/Hf and $W_{80}Ta_{20}$/Hf multilayer systems. The difference in the V_{Nernst} sign for amorphous W/Hf and $W_{80}Ta_{20}$/Hf multilayers is the same as that for crystalline W and $W_{80}Ta_{20}$ alloy systems.[17] Therefore, the current might mainly flow in the amorphous W and amorphous $W_{80}Ta_{20}$ in W/Hf and $W_{80}Ta_{20}$/Hf multilayer systems.

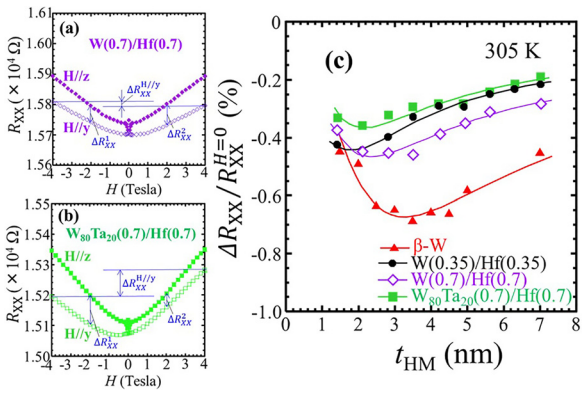

FIG. 3. Typical longitudinal resistance R_{xx} vs external magnetic field H oriented along the y axis (open symbols) and z axis (closed symbols) measured at 305 K for (a) the device with the W(0.7)/Hf(0.7) multilayer and for (b) the device with the $W_{80}Ta_{20}$(0.7)/Hf(0.7) multilayer. SMR $\Delta R_{XX}/R_{XX}^{H=0}$ plotted against the HM layer thickness t_{HM} for β-W and amorphous W/Hf multilayers and $W_{80}Ta_{20}$/Hf multilayer systems. The solid lines show the fitting results using Eqs. (4) and (5).

In order to neglect the thermal (anomalous Nernst) effect to analyze the SMR, we define the SMR by

$$\mathrm{SMR} = \Delta R_{XX}/R_{XX}^{H=0} = [\Delta R_{XX}^{1} + \Delta R_{XX}^{2}]/2R_{XX}^{H=0}, \quad (1)$$

$$\Delta R_{XX}^{1} = R_{XX}(H_y = -1.6\,\mathrm{T}) - R_{XX}(H_Z = -1.6\,\mathrm{T}), \quad (2)$$

$$\Delta R_{XX}^{2} = R_{XX}(H_y = +1.6\,\mathrm{T}) - R_{XX}(H_Z = +1.6\,\mathrm{T}), \quad (3)$$

where $R_{XX}^{H=0}$ is the longitudinal resistance at $H = 0$ T. Because we consider that the slight increase in ΔR_{XX} with increasing $|H|$ above 1.6 T may originate from the contribution of the Hanle magnetoresistance,[27,28] which causes an increase in R_{XX} ($|H_Z| \geq 1.6$ T) with increasing $|H|$ and enhancement of ΔR_{XX}, therefore, we used the values of R_{XX} at $|H| = 1.6$ T, which is the saturation magnetic field value for CoFeB in the magnetic hard-axis direction, for the estimation of SMR.

Figure 3(c) shows $\Delta R_{XX}/R_{XX}^{H=0}$ as a function of t_{HM} for β-W, W(0.35)/Hf(0.35), W(0.7)/Hf(0.7), and $W_{80}Ta_{20}$(0.7)/Hf(0.7) multilayer systems. The solid lines in Fig. 3(c) are the results fitting the measured data using the following equations:[19,23]

$$\mathrm{SMR} = \Delta R_{XX}/R_{XX}^{H=0} \sim \theta_{SH}^2 \frac{\lambda_S}{t_{HM}} \frac{\tanh(t_{HM}/2\lambda_S)}{1+\xi}\left[1 - \frac{1}{\cosh(t_{HM}/\lambda_S)}\right], \quad (4)$$

$$\xi \equiv \frac{\rho_{HM} t_{CoFeB}}{\rho_{CoFeB} t_{HM}}, \quad (5)$$

where λ_S is the spin diffusion length and $\rho_{CoFeB} = 139.9$ $\mu\Omega$ cm and ρ_{HM} are the resistivity determined by the fitting shown in Figs. 1(d) and 1(e). As shown in Fig. 3(c), the thickness values at which the maximum magnitude of $\Delta R_{XX}/R_{XX}^{H=0}$ for the fitted solid lines in the amorphous W/Hf multilayer and $W_{80}Ta_{20}$/Hf multilayer systems are thinner than those for β-W systems. This indicates that the λ_S values in amorphous W/Hf multilayer systems are lower than those in β-W systems. The applied SMR model is based on the drift diffusion model,[29] and therefore, the estimated θ_{SH} and the λs are all effective values. The magnitudes of $|\theta_{SH}|$ and λ_S of the β-W and amorphous W/Hf multilayer HM electrodes are successfully obtained.

Figures 4(a) and 4(b) show the results of the magnitudes of $|\theta_{SH}|$, σ_{SH}, and λ_S for β-W, amorphous W/Hf multilayers, and amorphous $W_{80}Ta_{20}$/Hf multilayers systems, respectively. The values of θ_{SH} for amorphous W/Hf multilayers and amorphous $W_{80}Ta_{20}$/Hf multilayers

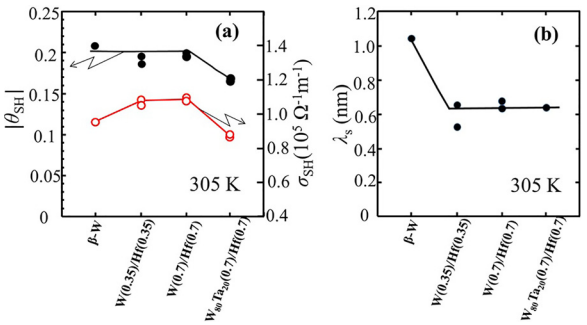

FIG. 4. (a) Estimated magnitude of the spin Hall angle $|\theta_{SH}|$ and spin Hall conductivity (σ_{SH}) and (b) spin diffusion length for the β-W, amorphous W/Hf multilayer, and amorphous $W_{80}Ta_{20}$/Hf multilayer systems. Black and red solid lines in (a) and (b) are given as guides to the eye.

are about −0.2 and −0.17. We found that the magnitude of $|\theta_{SH}|$ for amorphous W/Hf multilayers is nearly the same as that for β-W ($\theta_{SH} = -0.207$). The value of λs for amorphous W/Hf multilayers and amorphous $W_{80}Ta_{20}$/Hf multilayer is ∼0.64 nm and lower than the estimated value of β-W ($\lambda s = 1.05$ nm). The values of θ_{SH} and λs in β-W are consistent with the previous report.[23] The decrease in λs for the amorphous W/Hf multilayer and the amorphous $W_{80}Ta_{20}$/Hf multilayer would be related to the increase in the interfacial scattering of the multilayer system. Thus, we found that the magnitudes of $|\theta_{SH}|$ and σ_{SH} for the devices with amorphous W/Hf multilayers are nearly the same and larger than those for β-W, respectively, as shown in Fig. 4(a), even though the resistivity of amorphous W/Hf multilayers is smaller than that of β-W as shown in Fig. 1(e). This result suggests that amorphous W has potential to have a large SHE and low resistivity compared to β-W. When the film thickness ratio between W and Hf is optimized, further improvement in these characteristics might be expected. We would continue our efforts to optimize the film thickness ratio in the future.

Finally, we would like to discuss about whether post-annealing causes any significant interdiffusion or not in the multilayer systems. From the HR-TEM, it was difficult to conclude whether post-annealing causes any significant interdiffusion or not because the masses of the atoms are nearly the same between Hf and W (both metals are HMs). Therefore, we try to measure low-angle x-ray reflection for the as-deposited and 573 K annealed W(0.7)/Hf(0.7), $W_{80}Ta_{20}$(0.7)/Hf(0.7) and W(0.35)/Hf(0.35) multilayers (see the supplementary material). The low-angle x-ray reflection patterns show oscillations in the reflection intensity for both the as-deposited and annealed samples. The intensity of the oscillations slightly decreases for the $(W(0.35)/Hf(0.35))_{10}$ multilayers. This might be due to the interdiffusion between W and Hf layers. These oscillations can be better explained by assuming multilayer films; however, these patterns can also be explained when we assume perfect reflection from the flat monolayer film with about 6 nm. Therefore, from low-angle x-ray reflection patterns as well as HR-TEM, it would be difficult to conclude whether interdiffusion between Hf and W has occurred during annealing. This might be because W and Hf have similar mases. As we wrote before, we confirmed that the sample has (i) the amorphous structure of W/Hf multilayers, (ii) the flat interface between heavy metals and CoFeB, and (iii) highly (100) texture of MgO (1.0 nm) on CoFeB for even the W(0.7)/Hf(0.7) multilayer sample annealed at 673 K. W is easy to crystallize when the thickness of W is thicker than ∼3 nm. Therefore, we would like to emphasize that it is meaningful that amorphous W (a-W) with a large SHE and low resistivity can be formed to a thick thickness region by the insertion of amorphous Hf (a-Hf). Moreover, we confirmed that the magnetic properties shown in Figs. 2(a) and 2(b) are almost the same between the 573 K annealed samples and the 673 K annealed samples. Therefore, we believe that post-annealing does not cause significant interdiffusion.

In conclusion, by applying an artificially synthesized W/Hf multilayer/CoFeB/MgO system, a higher SHE and enhancement of $K_{eff}\,t^*$ can be achieved compared to the β-W/CoFeB/MgO system. In addition, the resistivity in the amorphous W/Hf multilayer is low compared to that in β-W. This study suggests that the artificially synthesized multilayer system is one of the avenues for realizing the HMs with a large SHE and low resistivity.

See the supplementary material for the results of low-angle x-ray reflection for the as-deposited and 573 K annealed W(0.7)/Hf(0.7), $W_{80}Ta_{20}$(0.7)/Hf(0.7), and W(0.35)/Hf(0.35) multilayers.

We thank T. Miyazaki for the measurement of HR-TEM images. This work was supported by the JST OPERA (No. JPMJOP1611) and JSPS KAKENHI (No. 19H00844).

REFERENCES

[1]L. Liu, C.-F. Pai, Y. Li, H. W. Tseng, D. C. Ralph, and R. A. Buhrman, Science **336**, 555 (2012).
[2]G. Yu, P. Upadhyaya, Y. Fan, J. G. Alzate, W. Jiang, K. L. Wong, S. Takei, S. A. Bender, L.-T. Chang, Y. Jiang, M. Lang, J. Tang, Y. Wang, Y. Tserkovnyak, P. K. Amiri, and K. L. Wang, Nat. Nanotechnol. **9**, 548 (2014).
[3]W. Jiang, P. Upadhyaya, W. Zhang, G. Yu, M. B. Jungfleisch, F. Y. Fradin, J. E. Pearson, Y. Tserkovnyak, K. L. Wang, O. Heinonen, S. G. E. Velthuis, and A. Hoffmann, Science **349**, 283 (2015).
[4]P. P. J. Haazen, E. Mure, J. H. Franken, R. Lavrijsen, H. J. M. Swagten, and B. Koopmans, Nat. Mater. **12**, 299 (2013).
[5]A. Chernyshov, M. Overby, X. Liu, J. K. Furdyna, Y. Lyanda-Geller, and L. P. Rokhinson, Nat. Phys. **5**, 656 (2009).
[6]I. M. Miron, K. Garello, G. Gaudin, P.-J. Zermatten, M. V. Costache, S. Auffret, S. Bandiera, B. Rodmacq, A. Schuhl, and P. Gambardella, Nature **476**, 189 (2011).
[7]J. Kim, J. Sinha, M. Hayashi, M. Yamanouchi, S. Fukami, T. Suzuki, S. Mitani, and H. Ohno, Nat. Mater. **12**, 240 (2013).
[8]S. Fukami, T. Anekawa, C. Zhang, and H. Ohno, Nat. Nanotechnol. **11**, 621 (2016).
[9]K.-S. Lee, S.-W. Lee, B.-C. Min, and K.-J. Lee, Appl. Phys. Lett. **104**, 072413 (2014).
[10]K. Garello, C. O. Avci, I. M. Miron, M. Baumgartner, A. Ghosh, S. Auffret, O. Boulle, G. Gaudin, and P. Gambardella, Appl. Phys. Lett. **105**, 212402 (2014).
[11]C. Zhang, S. Fukami, H. Sato, F. Matsukura, and H. Ohno, Appl. Phys. Lett. **107**, 012401 (2015).
[12]M.-H. Nguyen, C.-F. Pai, K. X. Nguyen, D. A. Muller, D. C. Ralph, and R. A. Buhrman, Appl. Phys. Lett. **106**, 222402 (2015).
[13]S. V. Aradhya, G. E. Rowlands, J. Oh, D. C. Ralph, and R. A. Buhrman, Nano Lett. **16**, 5987 (2016).
[14]M. Baumgartner, K. Garello, J. Mendil, C. O. Avci, E. Grimaldi, C. Murer, J. Feng, M. Gabureac, C. Stamm, Y. Acremann, S. Finizio, S. Wintz, J. Raabe, and P. Gambardella, Nanotechnology **12**, 980 (2017).
[15]Y. Kato, Y. Saito, H. Yoda, T. Inokuchi, S. Shirotori, N. Shimomura, S. Oikawa, A. Tiwari, M. Ishikawa, M. Shimizu, B. Altansargai, H. Sugiyama, K. Koi, Y. Ohsawa, and A. Kurobe, Phys. Rev. Appl. **10**, 044011 (2018).

[16]H. Honjo, T. V. A. Nguen, T. Watanabe, T. Nasuno, C. Zhang, T. Tanigawa, S. Miura, H. Inoue, M. Niwa, T. Yoshiduka, Y. Noguchi, M. Yasuhira, A. Tamakoshi, M. Natsui, Y. Ma, H. Koike, Y. Takahashi, K. Furuya, H. Shen, S. Fukami, H. Sato, S. Ikeda, T. Hanyu, H. Ohno, and T. Endoh, in International Electron Device Meeting,Technical Digest (2019), Vol. 28, p. 5.
[17]Y. Saito, N. Tezuka, S. Ikeda, H. Sato, and T. Endoh, Appl. Phys. Exp. **12**, 053008 (2019).
[18]Y. Saito, N. Tezuka, S. Ikeda, H. Sato, and T. Endoh, AIP. Adv. **9**, 125312 (2019).
[19]J. Liu, T. Ohkubo, S. Mitani, K. Hono, and M. Hayashi, Appl. Phys. Lett. **107**, 232408 (2015).
[20]C.-F. Pai, L. Liu, Y. Li, H. W. Tseng, D. C. Ralph, and R. A. Buhrman, Appl. Phys. Lett. **101**, 122404 (2012).
[21]A. Ganguly, K. Kondou, H. Sukegawa, S. Mitani, S. Kasai, Y. Niimi, Y. Otani, and A. Barman, Appl. Phys. Lett. **104**, 072405 (2014).
[22]Y. Wang, P. Deorani, X. Qiu, J. H. Kwon, and H. Yang, Appl. Phys. Lett. **105**, 152412 (2014).
[23]J. Kim, P. Sheng, S. Takahashi, S. Mitani, and M. Hayashi, Phys. Rev. Lett. **116**, 097201 (2016).
[24]C. Zhang, S. Fukami, K. Watanabe, A. Ohkawara, S. DuttaGupta, H. Sato, F. Matsukura, and H. Ohno, Appl. Phys. Lett. **109**, 192405 (2016).
[25]L. Wang, R. J. H. Wesselink, Y. Liu, Z. Yuan, K. Xia, and P. J. Kelly, Phys. Rev. Lett. **116**, 196602 (2016).
[26]C.-F. Pai, M.-H. Nguyen, C. Belvin, L. H. Vilela-Leão, D. C. Ralph, and R. A. Buhrman, Appl. Phys. Lett. **104**, 082407 (2014).
[27]M. I. Dyakonov, Phys. Rev. Lett. **99**, 126601 (2007).
[28]S. Velez, V. N. Golovach, A. Bedoya-Pinto, M. Isasa, E. Sagasta, M. Abadia, C. Rogero, L. E. Hueso, F. S. Bergeret, and F. Casanova, Phys. Rev. Lett. **116**, 016603 (2016).
[29]V. P. Amin and M. D. Stiles, Phys. Rev. B **94**, 104420 (2016).